

DARK MATTER HALO MASS PROFILES

DAN COE¹
Draft

ABSTRACT

I provide notes on the NFW, Einasto, Sérsic, and other mass profiles which provide good fits to simulated dark matter halos (§3). I summarize various published $c(M)$ relations: halo concentration as a function of mass (§1). The definition of the virial radius is discussed and relations are given to convert c_{vir} , M_{vir} , and r_{vir} between various defined values of the halo overdensity (§2).

Subject headings: cosmology: dark matter — galaxies: clusters: general — methods: data analysis — gravitational lensing

1. MASS-CONCENTRATION RELATIONS

The mass profiles of galaxy clusters appear to be more centrally concentrated than realized in simulations (Broadhurst et al. 2008; Oguri et al. 2009; Sereno et al. 2010). If true, this may be evidence for Early Dark Energy (see e.g., Grossi & Springel 2009). Or perhaps there is a less exciting explanation (e.g., Barkana & Loeb 2009; Lapi & Cavaliere 2009; Meneghetti et al. 2010). For more details, see my discussion in Coe et al. (2010). More conclusive results are expected from the CLASH HST MCT project² and perhaps LoCuSS (Okabe et al. 2009; Richard et al. 2009).

More massive halos generally have lower concentrations than less massive halos. This is seen in both simulations and observations, though less clearly so far in the latter (see below). More massive halos form later, resulting in lower concentrations reflecting the lower background density at the time of formation Navarro et al. (1996).

For a given radial mass profile (see §3), the concentration is defined as:

$$c_{vir} = r_{vir}/r_{-2}, \quad (1)$$

a mishmash ratio of the virial radius r_{vir} and the radius r_{-2} at which $\rho \propto r^{-2}$. For an NFW profile, $r_{-2} = r_s$. The definition of the virial radius r_{vir} is discussed at length in §2, but it is typically approximated as the region within which there is an average overdensity of a certain value ($\Delta_c \sim 100$ or 200) above ρ_{crit} . For clarity, one may quote the exact value of Δ_c used: c_{200} , for example.

In principle concentrations could be derived using any radial fitting profile (§3). However the choice does matter as the profiles behave differently between r_{-2} and r_{vir} . Concentrations derived from NFW and Einasto fits to the same halos (Duffy et al. 2008) are compared in Fig. 8. Einasto $c(M)$ relations have been derived for the Millennium simulation relaxed (Gao et al. 2008) and all Hayashi & White (2008) halos. Below we focus on $c(M)$ relations derived from NFW fits.

1.1. Current $c(M)$ measurements from NFW profile fits

The current best estimates for $c(M, z)$ are probably those given by Duffy et al. (2008) and Macciò et al. (2008). Their findings are similar. Both analyze simulations which use the WMAP5 cosmology, resulting in $\sim 20\%$ lower concentrations than WMAP1 (Table 8) as used in the Millennium simulation (Neto et al. 2007), for example. Duffy et al. (2008) find that present-day ($z = 0$) halos follow the following mass-concentration relation:

$$c_{200} \simeq 5.74 \left(\frac{M_{200}}{2 \times 10^{12} h^{-1} M_{\odot}} \right)^{-0.097}. \quad (2)$$

They provide a separate relation for relaxed clusters which are more symmetric and thus better fit by radial profiles such as NFW. These have 15 – 20% higher concentrations (Fig. 7):

$$c_{200} \simeq 6.67 \left(\frac{M_{200}}{2 \times 10^{12} h^{-1} M_{\odot}} \right)^{-0.092}. \quad (3)$$

Intrinsic scatters are $\Delta \log_{10}(c_{200}) \simeq 0.15$. These relations are plotted in Fig. 2 along with corresponding relations from Macciò et al. (2008).

Duffy et al. (2008) also supply fitted functions to halos spanning the redshift range $z = 0 - 2$. Full:

$$c_{200} \simeq \frac{5.71}{(1+z)^{0.47}} \left(\frac{M_{200}}{2 \times 10^{12} h^{-1} M_{\odot}} \right)^{-0.097} \quad (4)$$

and relaxed:

$$c_{200} \simeq \frac{6.71}{(1+z)^{0.44}} \left(\frac{M_{200}}{2 \times 10^{12} h^{-1} M_{\odot}} \right)^{-0.092}. \quad (5)$$

In their Table 1, they provide uncertainties for these fit parameters as well as corresponding values for c_{vir} and M_{vir} . These $c_{200}(M_{200}, z)$ relations are plotted in Figs. 3 & 4. Also plotted are the corresponding $c_{vir}(M_{vir}, z)$ relations provided by (Duffy et al. 2008). In Fig. 4, we plot the Bullock et al. (2001) $c \propto (1+z)^{-1}$ scaling for comparison. Note that Duffy08 find weaker dependencies on redshift: $c_{200} \propto (1+z)^{-0.45}$; $c_{vir} \propto (1+z)^{-0.70}$.

¹ Jet Propulsion Laboratory, California Institute of Technology, 4800 Oak Grove Dr, MS 169-327, Pasadena, CA 91109

² Cluster Lensing And Supernova survey with Hubble, <http://www.stsci.edu/~postman/CLASH/>

Halo concentrations are sensitive to cosmology. A higher σ_8 causes halos to form earlier, resulting in higher concentrations. This was the case in the Millennium simulations which used the WMAP 1-year cosmology, including $\sigma_8 = 0.9$. This yields concentrations $\sim 20\%$ higher than found in simulations which use WMAP5's $\sigma_8 = 0.796^3$ (Duffy et al. 2008). The effect of cosmology was explored in more detail by Macciò et al. (2008). These effects are shown in Fig. 5.

Various derived $c(M)$ relations (for $z = 0$) are plotted in Fig. 6. In our Tables 3, 4, and 5, we provide $c_{200}(M_{200})$, $c_{vir}(M_{vir})$, and $c(M, z)$ relations, respectively, as derived by Duffy et al. (2008), Macciò et al. (2008), Neto et al. (2007), Bullock et al. (2001), Hennawi et al. (2007), and Gentile et al. (2007).⁴ The latter is the original NFW $c(M)$ prescription updated to the WMAP3 cosmology.

The various simulations considered here are outlined in Table 7. The relevant details of their adopted cosmologies (Ω_m, σ_8) are given in Table 8. We provide the range of halo masses produced in each simulation. The dangers of extrapolating $c(M)$ relations beyond these ranges have been cited by Zhao et al. (2003), for example.

Neto et al. (2007, their Fig. 5) find that 10,000 particles within the virial radius are required to yield robust concentration measurements. They note that using fewer particles introduces scatter but does not appear to introduce bias in their concentration measurements.

Hennawi et al. (2007) measure significantly larger concentrations for galaxy clusters in their simulations. Their cluster concentrations are $\sim 50\%$ and $\sim 80\%$ larger than found by Duffy et al. (2008) and Macciò et al. (2008), respectively (Fig. 6, *right*). Their use of $\sigma_8 = 0.95$ probably only results in concentrations inflated by $\sim 20\%$ compared to the WMAP5 $\sigma_8 = 0.796$ simulations. The remaining disagreement may be a result of their halo density fitting procedure which they claim is better for comparison with lensing measurements. Specifically, they assign large uncertainties to radial bins with large subhalos. This may bias the fitted profiles to be low at large radius (where large subhalos typically reside) resulting in higher concentrations. These results may considerably ease tensions between observed and simulated halo concentrations. The differences in fitting procedure should be better studied and understood.

1.2. Care in citing concentration expectations

A concern often noted is that the concentration measured for A1689 (in every study to date) is higher than that found in simulations for a halo of A1689's mass. The concentration found in simulations has been cited loosely as $c \sim 5$ or $c \sim 5.5$ using a relation given by Bullock et al. (2001):

$$c_{vir} \simeq \frac{9}{1+z} \left(\frac{M_{vir}}{1.3 \times 10^{13} h^{-1} M_\odot} \right)^{-0.13}, \quad (6)$$

³ This value is in excellent agreement with the WMAP 7-year maximum likelihood value $\sigma_8 = 0.803$ (Komatsu et al. 2010).

⁴ I'll take a crack at completeness, and mention other papers with $c(M)$ relations neglected here (for no particular reason): Eke et al. (2001); Wechsler et al. (2002); Alam et al. (2002); Zhao et al. (2003); Dolag et al. (2004); Kuhlen et al. (2005); Lu et al. (2006); Shaw et al. (2006); Dutton et al. (2007); Gnedin et al. (2007). And I have probably missed still others!

But the expected concentration is actually lower ($c_{200} \sim 3.0$, exacerbating the disagreement with observations) for four reasons:

- $c_{200} < c_{vir}$
- $z > 0$
- WMAP7 vs. WMAP1
- $M_{vir} \approx 1.4 \times 10^{15} M_\odot / h > 10^{15} M_\odot$

We also note that Bullock et al. (2001) did not simulate halos as massive as A1689, with their most massive halos weighing in at $M \sim 10^{14} M_\odot / h$.

1.3. The observed $c(M)$ relation

Based on a compilation of 62 published measurements (including 10 new measurements) of halo c_{vir} and M_{vir} , Comerford & Natarajan (2007) find the following relation (with a large scatter):

$$c_{vir} \simeq \frac{14.5 \pm 6.4}{1+z} \left(\frac{M_{vir}}{1.3 \times 10^{13} h^{-1} M_\odot} \right)^{-0.15 \pm 0.13}. \quad (7)$$

For clusters as massive as A1689, Comerford's relation converges toward that of Hennawi et al. (2007), the former being only slightly higher.

This and other observed $c(M)$ relations are shown in Fig. 6 and detailed in Table 6. The Comerford & Natarajan (2007) compilation includes both lensing and X-ray determinations of c and M , including the X-ray samples presented by Buote et al. (2007) and Schmidt & Allen (2007). Each of these papers presented their own $c(M)$ relation. A recent $c(M)$ relation from weak lensing of individual halos was presented by Okabe et al. (2009). And $c(M)$ derived from *stacked* weak lensing analyses were presented by Johnston et al. (2007) and Mandelbaum et al. (2008). It seems apparent that one should study a wide enough range of halo masses to obtain a confident $c(M)$ relation.

2. OVERDENSITY WITHIN THE VIRIAL RADIUS

Various conventions are used to define the virial mass and radius. We explain and show how to convert between different definitions.

2.1. Overdensity Definitions

The virial radius r_{vir} designates the edge of the halo. Within this radius, objects are supposed to be "virialized": gravitationally bound and settled into regular orbits. Outside this radius, objects are not in orbit although they may still be infalling. In practice, there is no sharp dividing line the two regions. And even if there were, it would be extremely difficult to discern observationally for a given massive body. Meanwhile, the objects we study are not always virialized. In fact, galaxy clusters are the largest bodies which have had time to virialize given the age of the universe. Thus some of the clusters we observe have virialized just recently, but many are still in the process of doing so.

Despite these complications, we can define a virial radius for a massive body based on theory and simulations. Early theoretical work (Peebles 1980) predicted

that a sphere of material will collapse if its density exceeds $1.686(1+z)$ times that of the background. After it collapses and virializes, the sphere will obtain an average density

$$\Delta_c \approx 18\pi^2 \approx 178 \quad (8)$$

times the critical density $\rho_{crit}(z)$ at that redshift, where

$$\rho_{crit} = \frac{3H^2(z)}{8\pi G}. \quad (9)$$

Cole & Lacey (1996) cited this as a theoretical result and then confirmed it in simulations.⁵

Navarro et al. (1996) adopted the nice round number of $\Delta_c = 200$, which has been used commonly ever since to allow for easy comparison between papers. But the $\Delta_c \approx 178$ result was obtained in an Einstein de-Sitter cosmology of $(\Omega_m, \Omega_\Lambda) = (1, 0)$. In the concordance cosmology $(\Omega_m, \Omega_\Lambda) = (0.3, 0.7)$, we find a much lower value of $\Delta_c \approx 100$, as we describe next.

At least three different forms have been given for Δ_c as a function of cosmology. For a flat universe ($\Omega_m + \Omega_\Lambda = 1$), Bryan & Norman (1998) give

$$\Delta_c \approx 18\pi^2 - 82\Omega_\Lambda - 39\Omega_\Lambda^2. \quad (10)$$

An approximation to this is given as (Eke et al. 1998)

$$\Delta_c \approx 178\Omega_m^{0.45}. \quad (11)$$

And Nakamura & Suto (1997, their Eq. C19; see also Henry 2000, their Eq. A17) give

$$\Delta_c \approx 18\pi^2(1 + 0.4093x^{2.7152})\Omega_m \quad (12)$$

with $x \equiv (1/\Omega_{m,0} - 1)^{1/3}(1+z)^{-1}$ and $\Omega_m(z) = 1/(1+x^3)$. Given the current concordance cosmology with $\Omega_m = 0.3$, these different expressions yield $\Delta_c = 101.1, 103.5, 100.3$, respectively for a halo at $z = 0$. Or given $\Omega_m = 0.25$, $\Delta_c = 94.2, 95.4, 93.5$. We note $\Omega_m = 0.25$ is in better agreement with the WMAP 7-year value (Komatsu et al. 2010) and $h = 0.742 \pm 0.036$ from Riess et al. (2009).

The overdensity is often quoted as a factor Δ_{vir} above the mean background density $\rho_m = \Omega_m \rho_{crit}$:

$$\rho_{halo} = \Delta_c \rho_{crit} = \Delta_{vir} \rho_m \quad (13)$$

With $\Delta_c = \Delta_{vir} \Omega_m$, $\Delta_c = 101.1$ corresponds to $\Delta_{vir} = 337$ for $\Omega_m = 0.3$. This value is cited by e.g., Bullock et al. (2001) and Graham et al. (2006). Using the Eke et al. (1998) relation and the Spergel et al. (2003) first-year WMAP value of $\Omega_m = 0.268$, Merritt et al. (2006, among others) give $\Delta_{vir} = 368$.

To facilitate comparison among current and future investigations, we propose that a value of $\Delta_c = 100$ be adopted for present-day halos. This corresponds to $\Delta_{vir} = 333$ given $\Omega_m = 0.3$, or the nice round number $\Delta_{vir} = 400$ given $\Omega_m = 0.25$. We also note that for $\Omega_m = 0.25$, the Bryan & Norman (1998) expression yields $\Delta_c \approx 94$, $\Delta_{vir} \approx 376$.

⁵ Cole & Lacey (1996) spoke of this factor as the overdensity above $\rho_m = \Omega_m \rho_{crit}$ rather than above ρ_{crit} . But as $\Omega_m = 1$ in their simulations, the two densities were equal and thus interchangeable.

While results from simulations are most often reported for present-day halos, Nature provides us observers with images of clusters as they were in the past. Thus in the expressions above, we should replace the present day values of $\Omega_{m,0}$ and $\Omega_{\Lambda,0}$ (here “0” subscripts have been added for clarity) with:

$$\Omega_m(z) = \frac{1}{1 + (\Omega_{\Lambda,0}/\Omega_{m,0})(1+z)^{-3}} \quad (14)$$

and $\Omega_\Lambda(z) = 1 - \Omega_m(z)$. For the massive galaxy cluster A1689 at $z = 0.1862$ and adopting $\Omega_m = 0.3$, the widely used Bryan & Norman (1998) expression yields $\Delta_c = 116.6$ and the Nakamura & Suto (1997) expression yields $\Delta_c = 115$. The latter was adopted by Broadhurst et al. (2005a,b, private communication) so we adopt it as well for consistency in Coe et al. (2010).

In Figs. 13, 14, and 15, we plot $\Omega_m(z)$, $\Delta_c(z)$, and $\Delta_{vir}(z)$.

2.2. Conversion between overdensity values Δ_c

If the mass profile is well described by an NFW profile, then it is straightforward to convert c_{vir} , r_{vir} , and M_{vir} between different conventions of Δ_c (c.f., Fig. 8). Converting from c_{200} ($\Delta_c = 200$) to c_{115} ($\Delta_c = 115$), for example, simply involves finding that value of c_{115} which yields the same value of δ_c (Eq. 38) as did c_{200} . This can be accomplished by a simple root finding program, but the relation is very linear as shown in Fig. 9. Here we provide expressions

$$c_{94} \approx 1.328c_{200} + 0.272 \quad (15)$$

$$c_{100} \approx 1.298c_{200} + 0.246 \quad (16)$$

$$c_{115} \approx 1.232c_{200} + 0.189 \quad (17)$$

which are accurate to within 0.5% for $2 < c_{200} < 25$.

These factors may be generalized:

$$c_{vir} \approx a c_{200} + b \quad (18)$$

$$a \approx -1.119 \log_{10} \Delta_c + 3.537 \quad (19)$$

$$b \approx -0.967 \log_{10} \Delta_c + 2.181 \quad (20)$$

to yield c_{vir} within 1% for $3 < c_{200}$ and $70 < \Delta_c < 140$. These factors are plotted in Fig. 10.

An alternate expression gives c_{vir} as a function of c_{200} and Δ_c :

$$c_{vir} = c_{200} + c_{200}^{0.9} 10^p \quad (21)$$

$$p = -(8.683 \times 10^{-5}) \Delta_c^{1.82} \quad (22)$$

to within 1% for $3 < c_{200} < 35$ and $85 < \Delta_c < 165$ ($z < 1$ or so).

See also Hu & Kravtsov (2003, Appendix C).

2.3. Virial Mass

Virial mass (the mass within r_{vir}) is given by

$$M_{vir} = \frac{4}{3} \pi r_{vir}^3 \Delta_c \rho_{crit}(z) = \frac{r_{vir}^3 \Delta_c H^2(z)}{2G} \quad (23)$$

In Fig. 12 we plot this simple relation between r_{vir} and M_{vir} .

Quoted values for M_{200} and r_{200} can also be converted to M_{vir} and r_{vir} as a function of c_{200} and Δ_c as plotted in Fig. 11. For a given NFW curve (with fixed r_s and ρ_s), r_{vir} simply scales with c_{vir} since r_s stays fixed. So $r_{vir}/r_{200} = c_{vir}/c_{200}$. As for the M_{vir} conversions, we solved for those numerically.

3. MASS PROFILES

3.1. Double Power Laws

In dark matter simulations, galaxy and cluster halos Navarro et al. (1996, 1997) were all shown to have mass density profiles well approximated by the NFW profile:

$$\rho(r) = \frac{\rho_s}{(r/r_s)(1 + r/r_s)^2}. \quad (24)$$

This profile behaves as $\rho \propto r^{-1}$ in the core, $\rho \propto r^{-2}$ at $r = r_s$, and steepens to $\rho \propto r^{-3}$ in the outskirts. The two fit parameters ρ_s and r_s were shown to be related and a function of halo mass. This ‘‘universal’’ profile is still a good approximation to today’s simulated halos. However the higher resolution does reveal subtle differences.

Deviations were sought for using a generalized version of the NFW profile (Hernquist 1990, his Eq. 43; see also Zhao 1996; Wytthe et al. 2001):

$$\rho(r) = \frac{2^{(\beta-\gamma)/\alpha} \rho_s}{(r/r_s)^\gamma [1 + (r/r_s)^\alpha]^{(\beta-\gamma)/\alpha}}. \quad (25)$$

This profile behaves as $\rho \propto r^{-\gamma}$ in the core, and $\rho \propto r^{-\beta}$ in the outskirts. The rate of transition is governed by α . Where NFW found $(\alpha, \beta, \gamma) = (1, 3, 1)$, Moore et al. (1999) instead found best fits of (1.5, 3, 1.5). Importantly, the inner profile was steeper: $\gamma = 1.5$, $\rho \propto r^{-1.5}$. There were many other attempts to accurately resolve and measure this inner slope, including Diemand et al. (2005) who found $\rho \propto r^{-1.2}$.

The fully generalized form in Equation 25 proves a bit too general with large degeneracies between the free parameters (Klypin et al. 2001). Thus, in their efforts to determine the central slope γ , authors often use one of two constrained versions of Equation 25, either a ‘‘generalized NFW’’ profile with $(\alpha, \beta, \gamma) = (1, 3, \gamma)$:

$$\rho(r) = \frac{2^{3-\gamma} \rho_s}{(r/r_s)^\gamma [1 + (r/r_s)^{(3-\gamma)}]}, \quad (26)$$

or what we might call a ‘‘generalized Moore’’ profile⁶ with $(\alpha, \beta, \gamma) = (3 - \gamma, 3, \gamma)$:

$$\rho(r) = \frac{2\rho_s}{(r/r_s)^\gamma [1 + (r/r_s)^{3-\gamma}]}. \quad (27)$$

Meanwhile, Dehnen & McLaughlin (2005) found $(\alpha, \beta, \gamma) = (4/9, 31/9, 7/9)$:

$$\rho(r) = \frac{2\rho_s^6}{(r/r_s)^{7/9} [1 + (r/r_s)^{4/9}]^6}. \quad (28)$$

⁶ This latter form is also often referred to as a ‘‘generalized NFW’’ profile, although strictly speaking it can only exactly reproduce the Moore profile and not that of NFW.

and when accounting for anisotropy, the more general $\{\alpha, \beta, \gamma\} = \{(3 - \gamma)/5, (18 - \gamma)/5, \gamma\}$:

$$\rho(r) = \frac{2\rho_s^6}{(r/r_s)^\gamma [1 + (r/r_s)^{(3-\gamma)/5}]^6}. \quad (29)$$

3.2. Continuously Varying Power Laws

The original NFW proponents proposed a new profile which gradually flattens all the way toward the center (Navarro et al. 2004). This profile was found (Navarro et al. 2004; Merritt et al. 2005, 2006) to yield better fits to a wide range of simulated dark matter halos than did the generalized NFW profile (Eq. 26), which has an equal number (3) of free parameters, including the central slope. Inner slopes as steep as $\rho(r) \propto r^{-1.2}$ are clearly ruled out by recent simulations (Navarro et al. 2010).

The new Navarro et al. (2004) fitting form was quickly recognized (Merritt et al. 2005) as the Sérsic (1968) profile generally applied to fitting the light distributions of elliptical galaxies. The implications are intriguing: that the collapse of massive bodies, be they luminous or dark matter, may lead to similar profiles.

However to be precise, Navarro et al. (2004) fit a Sérsic-like profile to 3-D density distributions, where the Sérsic profile was fit to 2-D surface density distributions (of light). Einasto (1965) was first to use such a density law to describe a 3-D distribution, namely the spatial distribution of old stars within the Milky Way.

Today we distinguish between the ‘‘Einasto’’ and ‘‘Sérsic’’ mass profiles. The former is fit to 3-D mass density $\rho(r)$ while the latter is fit to 2-D projected mass distributions $\Sigma(R)$. Projected and deprojected approximations to the Einasto and Sérsic profiles, respectively, have also been derived (see Table 1).

The Sérsic (1968) profile is given by:

$$\Sigma(R) = \Sigma_e \exp \left\{ -b_n \left[\left(\frac{R}{R_e} \right)^{1/n} - 1 \right] \right\}, \quad (30)$$

There are three free parameters: Σ_e , R_e , and n , with b_n being a function of n (given below) such that half the mass is contained within R_e . Note that the total mass of a Sérsic profile is finite, unlike that for an NFW profile. A 3-D deprojected approximation is given by Prugniel & Simien (1997).

The Einasto mass profile is a similar function but of 3-D mass density $\rho(r)$:

$$\rho(r) = \rho_{-2} \exp \left(-\frac{2}{\alpha} \left[\left(\frac{r}{r_{-2}} \right)^\alpha - 1 \right] \right) \quad (31)$$

where ρ_{-2} and r_{-2} are the density and radius at which $\rho(r) \propto r^{-2}$. The concentration is defined as $c_{vir} = r_{vir}/r_{-2}$. Navarro et al. (2010) found $\alpha \approx 0.17$ for galaxy-sized halos in the Aquarius simulation. Gao et al. (2008) concur and found α increases to ~ 0.3 for the most massive clusters in the Millennium simulation. Duffy et al. (2008) reduce the Einasto profile to two free parameter by using the ‘‘peak height’’ $\alpha(\nu)$ relation from Gao et al. (2008). A 2-D projected approximation of Einasto is given by Dhar & Williams (2010).

TABLE 1
SÉRSIC-LIKE PROFILES OF 2-D AND 3-D DENSITY

3-D $\rho(r)$		2-D $\Sigma(R)$
Einasto (1965)	<u>projected</u> \rightarrow	Dhar & Williams (2010)
Prugniel & Simien (1997)	\leftarrow <u>deprojected</u>	Sérsic (1968)

TABLE 2
3-PARAMETER FITS: DEVIATIONS FROM HALO
PROFILES MEASURED IN MERRITT ET AL.
(2006, THEIR TABLE 4)

Model	6 clusters	4 galaxies
Einasto	0.028	0.026
Prugniel-Simien ^a	0.025	0.030
generalized NFW	0.032	0.028
Dehnen-McLaughlin	0.034	0.023

^a deprojected Sérsic

Merritt et al. (2005, 2006) experimented with both of these and other fits to 3-D mass density profiles of simulated halos. In the latter paper, they compared the performance of various formulae fit to 10 simulated halos (6 cluster-sized and 4 galaxy-sized). Their results for 3-parameter fits are reprinted here in Table 2. The four tested profiles yielded similar results. Einasto performed a bit better across the board. Prugniel-Simien (the deprojected Sérsic profile) performed a bit better for clusters. Dehnen-McLaughlin performed a bit better for galaxies. And the generalized NFW profile (Eq. 26) was not far behind.

Given the small number of halos tested, and the similarity of the performances, all of these fitting formulae might still be considered reasonable choices. However the Einasto profile has become especially popular (e.g., Hayashi & White 2008; Gao et al. 2008; Duffy et al. 2008; Navarro et al. 2010).

Recently a new fitting formula was proposed by Stadel et al. (2009). It yields superior fits to the two high resolution halos tested (Via Lactea 2 and GHALO):

$$\rho(r) = \rho_0 e^{-\lambda[\ln(1+r/R_\lambda)]^2} \quad (32)$$

with $\lambda \simeq 0.1$.

3.3. Power Law Behaviors

Power law slopes for the above fitting formulae as a function of r are plotted in Figs. 16, 17, 18. The slopes were calculated numerically as $d \ln \rho / d \ln r$. For fun, we note this is equivalent to $(d\rho/dr)(r/\rho)$. The radii r are given in units of r_{-2} at which $\rho \propto r^{-2}$.

We see that in principle, we should be able to distinguish between these various profiles in both observed and simulated halos given sufficient resolution at a large enough range of radii. Such clear determinations have so far eluded us.

In Fig. 19, we plot power law slopes for $\rho(r)$, $\kappa(R)$, and $M(< R)$ for the NFW profile.

3.4. Profile Details

Here we provide useful expressions derived from the NFW and Sérsic profiles.

3.4.1. NFW Profile

Simulated galaxy and cluster halos Navarro et al. (1996, 1997) were shown to all have mass density profiles well approximated by the NFW profile:

$$\rho(r) = \frac{\rho_s}{(r/r_s)(1+r/r_s)^2}. \quad (33)$$

The two fit parameters ρ_s and r_s were shown to be related and a function of halo mass, as we discuss below. But the parameter making all the buzz these days is the central mass concentration:

$$c_{vir} = r_{vir}/r_s, \quad (34)$$

where r_{vir} is the virial radius of the mass halo. As discussed above, the virial radius is estimated as that which contains an average density $\Delta_c \rho_{crit}$, for a total virial mass of

$$M_{vir} = \frac{4}{3} \pi \Delta_c \rho_{crit} r_{vir}^3. \quad (35)$$

For an NFW halo, the mass within a sphere with radius $r = x r_s$ can be found by simply integrating the NFW profile (Eq. 33):

$$M(r) = 4\pi r_s^3 \int_0^x dx' x'^2 \frac{\rho_s}{x'(1+x')^2} \quad (36)$$

$$= 4\pi \rho_s r_s^3 \left(\ln(1+x) - \frac{x}{1+x} \right) \quad (37)$$

Combining Eqs. 34, 35, and 37, we find that the concentration parameter c can be obtained from the following expression, as given in Navarro et al. (1996):

$$\frac{\rho_s}{\rho_{crit}} \equiv \delta_c = \frac{\Delta_c}{3} \frac{c^3}{\ln(1+c) - c/(1+c)}. \quad (38)$$

To fit the NFW profile to our gravitational lensing mass maps which measure projected surface density, we integrate the NFW profile along the line of sight (e.g., Golse & Kneib 2002) to find the projected surface density:

$$\Sigma(R) = 2\rho_s r_s F(X) \quad (39)$$

with $R = X r_s$ and

$$F(X) = \begin{cases} \frac{1}{X^2 - 1} \left(1 - \frac{1}{\sqrt{1 - X^2}} \cosh^{-1} \frac{1}{X} \right) & (X < 1) \\ \frac{1}{3} & (X = 1) \\ \frac{1}{X^2 - 1} \left(1 - \frac{1}{\sqrt{X^2 - 1}} \cos^{-1} \frac{1}{X} \right) & (X > 1) \end{cases} \quad (40)$$

Integrating once more over the area within R , we find

the total mass within a *cylinder* of radius R

$$M(R) = 4\pi r_s^3 \rho_s G(X) \quad (41)$$

with

$$G(X) = \ln \frac{X}{2} + \begin{cases} \frac{1}{\sqrt{1-X^2}} \cosh^{-1} \frac{1}{X} & (X < 1) \\ 1 & (X = 1) \\ \frac{1}{\sqrt{X^2-1}} \cos^{-1} \frac{1}{X} & (X > 1) \end{cases} \quad (42)$$

This should not be confused with Eq. 37 which gives mass within a *sphere* of radius r .

From this we can obtain the shear due to an NFW mass profile: $\gamma(R) = \bar{\kappa}(R) - \kappa(R)$:

$$\gamma(R) = 2\kappa_s \left(\frac{2G(X)}{X^2} - F(X) \right). \quad (43)$$

The quantity measured in weak lensing studies is the reduced shear:

$$g = \frac{(D_{LS}/D_S)\gamma}{1 - (D_{LS}/D_S)\kappa}, \quad (44)$$

where we have finally given the redshift dependence. (All previous expressions were given for a fiducial lensed source at $z_s = \infty$.)

3.4.2. Sérsic Profile

We now give the Sérsic (1968) profile and quantities derived from it (e.g., Graham & Driver 2005; Terzić & Graham 2005). Note that the Sérsic profile is commonly used to describe the (projected 2-D) light profiles of elliptical galaxies. Here instead it will be discussed as describing projected mass profiles.

The Sérsic (1968) profile is given by:

$$\Sigma(R) = \Sigma_e \exp \left\{ -b_n \left[\left(\frac{R}{R_e} \right)^{1/n} - 1 \right] \right\}, \quad (45)$$

There are three free parameters: Σ_e , R_e , and n , with b_n being a function of n (given below) such that half the mass is contained within R_e . (Note that the total mass of a Sérsic profile is finite, unlike that for an NFW profile.) The total projected mass within a radius R is given as:

$$M(R) = 2\pi \Sigma_e R_e^2 n e^{b_n} b_n^{-2n} \hat{\gamma}(2n, x) \quad (46)$$

where

$$x = b_n (R/R_e)^{1/n}, \quad (47)$$

and $\hat{\gamma}(a, x) = \int_0^x dt e^{-t} t^{a-1}$ is the incomplete gamma function (with the ‘‘hat’’ used to distinguish $\hat{\gamma}$ from the lensing shear γ). Thus to satisfy $M(R_e) = \frac{1}{2}M(R = \infty)$, b_n must obey:

$$\Gamma(2n) = 2\hat{\gamma}(2n, b_n) \quad (48)$$

where $\Gamma(a) = \hat{\gamma}(a, \infty)$ is the complete gamma function. In SciPy’s ‘‘special’’ package, we find a routine to quickly

calculate $b_n = \text{gammaincinv}(2 * n, 0.5)$. An approximation may also be used (Prugniel & Simien 1997):

$$b_n \approx 2n - 1/3 + 0.009876/n \quad (49)$$

Lensing properties of the Sérsic profile have been derived and explored in Cardone (2004) and Elfasdóttir & Möller (2007). Of special interest here is the weak shear $\gamma = \bar{\kappa} - \kappa$. The average κ within R can be derived straightforwardly from the above expression for $M(R)$:

$$\bar{\kappa}(R) = \frac{M(R)}{\pi R^2 \Sigma_{crit}} = 2\kappa_e n e^{b_n} x^{-2n} \hat{\gamma}(2n, x) \quad (50)$$

where we have introduced $\kappa_e = \Sigma_e / \Sigma_{crit}$. Meanwhile, $\kappa(R) = \Sigma(R) / \Sigma_{crit}$ can be rewritten as:

$$\kappa(R) = \kappa_e e^{(b_n - x)} \quad (51)$$

Thus we find $\gamma(R) = \bar{\kappa}(R) - \kappa(R)$:

$$\gamma(R) = \kappa_e e^{b_n} (2n x^{-2n} \hat{\gamma}(2n, x) - e^{-x}), \quad (52)$$

with the reduced shear given as $g = (\gamma D_{LS}/D_S)/(1 - \kappa D_{LS}/D_S)$.

There are fewer published fits of Sérsic profiles to simulated cluster halos. We do note that Merritt et al. (2005) found $n = 2.38 \pm 0.25$ for their cluster sample.

We thank Angelo Neto for useful conversations about the Millennium simulation and their study of halo profiles. This work was carried out at Jet Propulsion Laboratory, California Institute of Technology, under a contract with NASA.

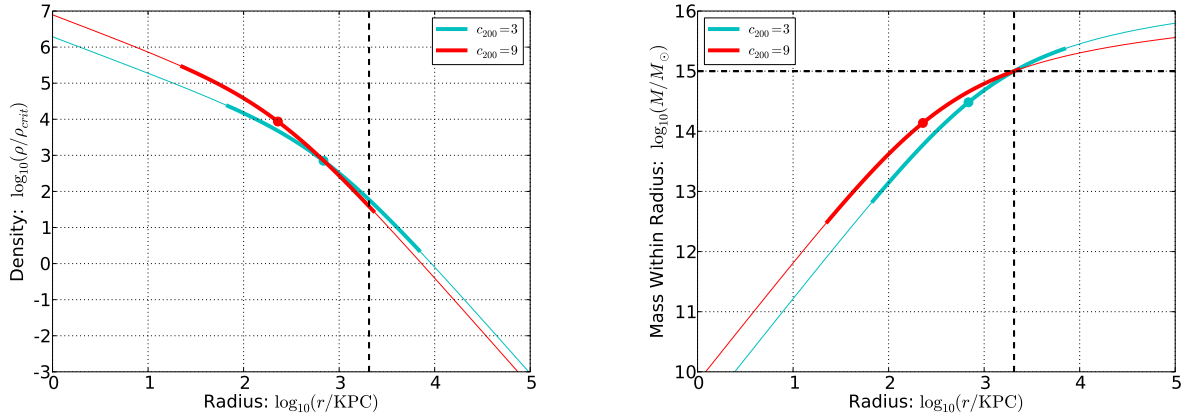


FIG. 1.— For fixed $M_{200} = 10^{15} M_{\odot}$, we show what an “over-concentrated” looks like: $c_{200} = 9$ versus the expected concentration ($c_{200} = 3$). This is roughly the case for A1689 (Coe et al. 2010). Dots mark r_s and dashed lines mark r_{vir} and M_{vir} . Thicker lines are used for two decades in radius about r_s to emphasize the shifting of the curves.

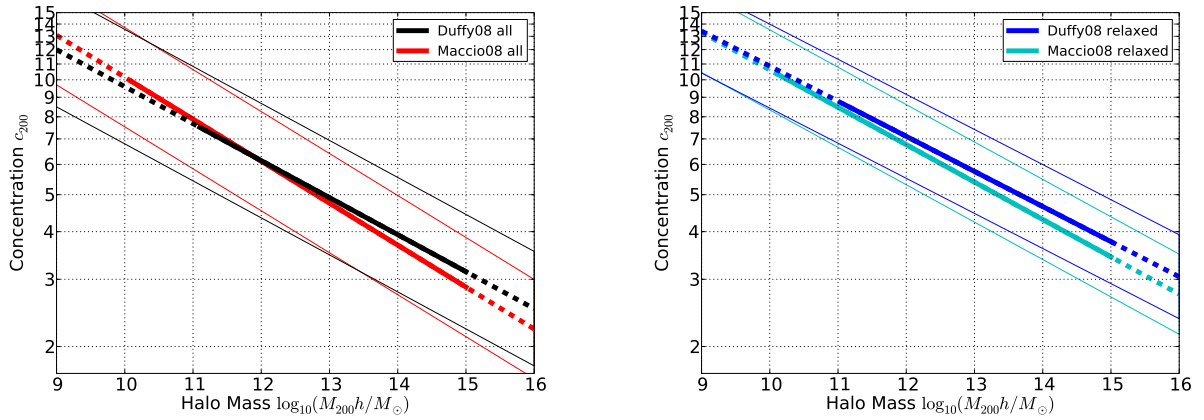


FIG. 2.— Expected NFW concentration c_{200} and $1-\sigma$ scatter as a function of halo mass M_{200} for all clusters (left) and relaxed clusters (right).

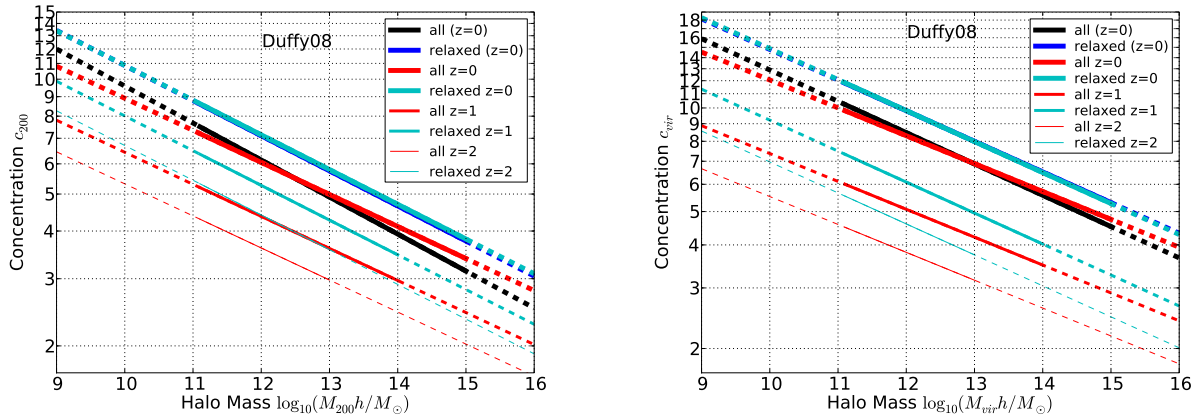


FIG. 3.— Expected NFW concentration $c(M)$ for $z = 0$ halos and $c(M, z)$ for $z = 0, 1, 2$ halos from Duffy et al. (2008).

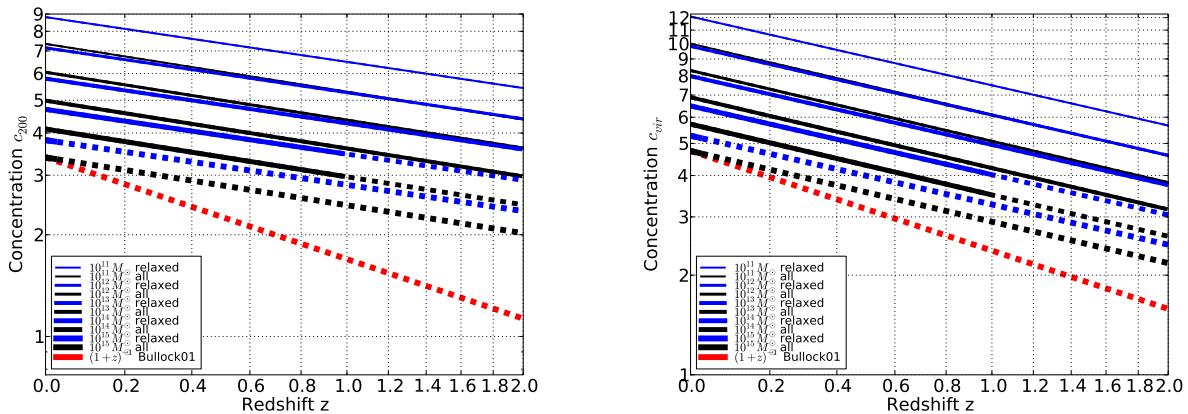


FIG. 4.— Expected NFW concentrations as a function of redshift for various mass halos from Duffy et al. (2008) (see Table 5). Also plotted is the $c \propto (1+z)^{-1}$ slope expected from Bullock et al. (2001). The x axes are plotted on scales of $\log(1+z)$.

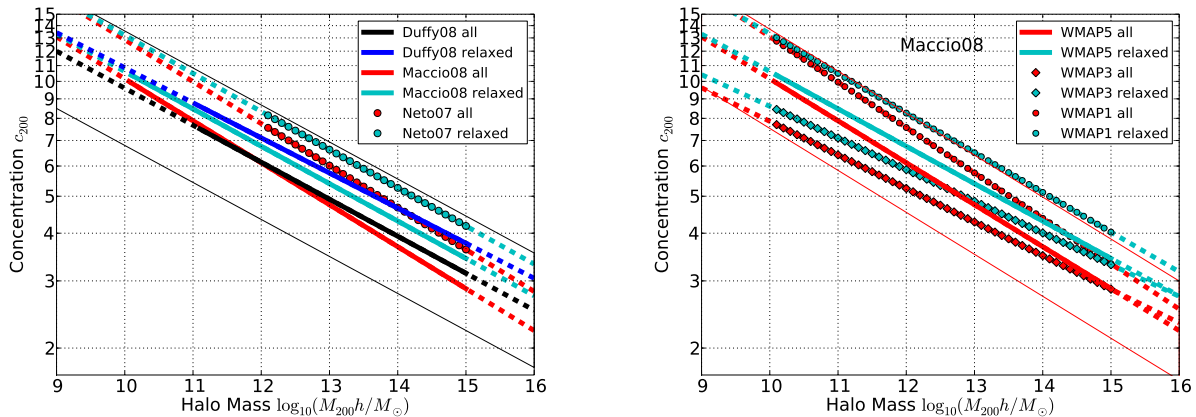


FIG. 5.— The effect of cosmology. Left: the Millennium simulation (Neto07) used WMAP1 with a higher σ_8 resulting in higher concentrations. Right: 3 different simulations with different cosmologies used.

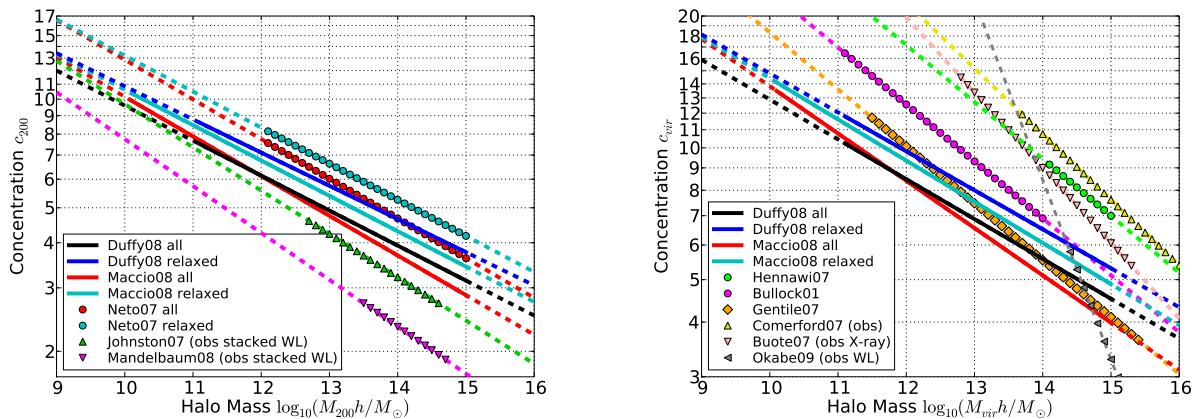


FIG. 6.— Comparing several studies, including both simulated and observed NFW $c(M)$.

TABLE 3
NFW $c_{200}(M_{200})$ FIT PARAMETERS ($z = 0$): $c_{200} = c_0(M_{200}/M_0)^{-\alpha} \pm \Delta c_{200}$

Sample		Cosmology	c_0	$M_0[M_\odot/h]$	α	$\Delta \log_{10} c_{200}$
Duffy08	all	WMAP5	5.74	2×10^{12}	0.097	0.15
Duffy08	relaxed	WMAP5	6.67	2×10^{12}	0.092	0.15
Maccio08	all	WMAP5	6.12	10^{12}	0.110	0.130
Maccio08	relaxed	WMAP5	6.76	10^{12}	0.098	0.105
Maccio08	all	WMAP3	5.24	10^{12}	0.088	0.132
Maccio08	relaxed	WMAP3	5.87	10^{12}	0.083	0.109
Maccio08	all	WMAP1	7.57	10^{12}	0.119	0.129
Maccio08	relaxed	WMAP1	8.26	10^{12}	0.104	0.111
Neto07	all	WMAP1	4.67	10^{14}	0.11	0.094
Neto07	relaxed	WMAP1	5.26	10^{14}	0.10	0.061

TABLE 4
NFW $c_{vir}(M_{vir})$ FIT PARAMETERS ($z = 0$): $c_{vir} = c_0(M_{vir}/M_0)^{-\alpha} \pm \Delta c_{vir}$

Sample		Cosmology	c_0	$M_0[M_\odot/h]$	α	$\Delta \log_{10} c_{vir}$
Duffy08	all	WMAP5	7.96 ± 0.17	2×10^{12}	0.091 ± 0.007	...
Duffy08	relaxed	WMAP5	9.23 ± 0.15	2×10^{12}	$0.089^{+0.010}_{-0.013}$...
Maccio08	all	WMAP5	8.41	10^{12}	0.108	...
Maccio08	relaxed	WMAP5	9.35	10^{12}	0.094	...
Maccio08	all	WMAP3	7.26	10^{12}	0.086	...
Maccio08	relaxed	WMAP3	8.22	10^{12}	0.080	...
Maccio08	all	WMAP1	10.26	10^{12}	0.114	...
Maccio08	relaxed	WMAP1	11.25	10^{12}	0.099	...
Hennawi07	all	WMAP1	12.3	1.3×10^{13}	0.13	0.098
Gentile07	all	WMAP3	13.6	10^{11}	0.13	...
Bullock01	all	WMAP1	9	1.3×10^{13}	0.13	0.14 ^a
Comerford07	all	observed	14.5 ± 6.4	1.3×10^{13}	0.15 ± 0.13	0.15

^a Wechsler et al. (2002, footnote 10) claim that the scatter of $\Delta \log_{10} c_{vir} = 0.18$ reported by Bullock et al. (2001) was a bit too high and should actually be 0.14, thus bringing it in line with their own measured scatter.

TABLE 5
NFW $c(M, z)$ FIT PARAMETERS FOR $0 < z < 2$: $c = c_0(M/M_0)^{-\alpha}(1+z)^{-\beta}$

Sample		Cosmology	Δ	c_0	$M_0[M_\odot/h]$	α	β
Duffy08	all	WMAP5	200	5.71 ± 0.12	2×10^{12}	0.084 ± 0.006	0.47 ± 0.04
Duffy08	relaxed	WMAP5	200	6.71 ± 0.12	2×10^{12}	0.091 ± 0.009	0.44 ± 0.05
Duffy08	all	WMAP5	vir	$7.85^{+0.17}_{-0.18}$	2×10^{12}	0.081 ± 0.006	0.71 ± 0.04
Duffy08	relaxed	WMAP5	vir	$9.23^{+0.17}_{-0.16}$	2×10^{12}	0.090 ± 0.009	0.69 ± 0.05

TABLE 6
OBSERVED $c(M)$ FIT PARAMETERS ($z = 0$): $c = c_0(M/M_0)^{-\alpha}(1+z)^{-\beta}$

Sample	Analysis	Δ_c	c_0	M_0 [$h^{-1}M_\odot$]	α	$\Delta \log_{10} c$	N	M_{\min} [$h^{-1}M_\odot$]	M_{\max} [$h^{-1}M_\odot$]	z
Comerford07 ^b	compilation	vir	14.5 ± 6.4	1.3×10^{13}	0.15 ± 0.13	0.15	62	5×10^{13}	4×10^{15}	0.003 – 0.89
Buote07	X-ray	vir	9.0 ± 0.4	10^{14}	0.172 ± 0.026	...	39 relaxed	6×10^{12}	2×10^{15}	0.0033 – 0.2302
SchmidtAllen07	X-ray	vir	7.55 ± 0.90^c	8×10^{14}	0.45 ± 0.12^c	...	34 relaxed	2×10^{14}	4×10^{15}	0.06 – 0.7
Okabe09	WL	vir	$8.45^{+3.91}_{-2.80}$	10^{14}	0.41 ± 0.19	0.19	30	2×10^{14}	1.5×10^{15}	0.15 – 0.30
Johnston07	stacked WL	200	4.1 ± 1.2	1.3×10^{13}	0.12 ± 0.04	...	130,000	5×10^{12}	5×10^{14}	~ 0.25
Mandelbaum08 ^d	stacked WL	54	4.6 ± 0.7	10^{14}	0.13 ± 0.07	...	222,699	3×10^{13}	6×10^{14}	~ 0.22
Mandelbaum08 ^e	stacked WL	200	2.5 ± 0.4	6×10^{13}	0.13 ± 0.07	...	222,699	3×10^{13}	6×10^{14}	~ 0.22

NOTE. — SchmidtAllen07 find $\beta = 0.71 \pm 0.52^c$, but all others fix $\beta = 1$ while fitting only (c_0, α) .

^b Includes Buote07 and SchmidtAllen07

^c Quoted uncertainties are 95% rather than 1- σ

^d Mandelbaum08 used $\Delta_{vir} = 200$ (not $\Delta_c = 200$) and assumed $\Omega_m = 0.27$, corresponding to $\Delta_c = \Omega_m \Delta_{vir} = 54$.

^e Converted from previous line

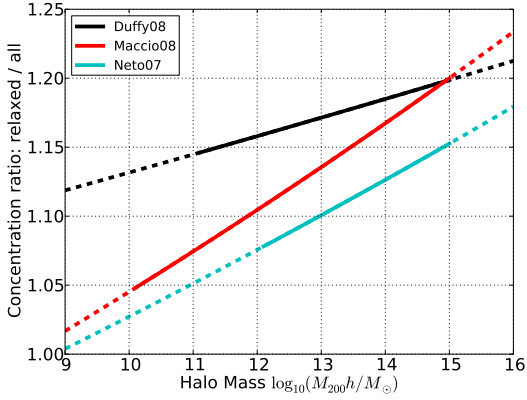


FIG. 7.— Ratio of NFW c_{200} for relaxed vs. all $z = 0$ halos in various simulations.

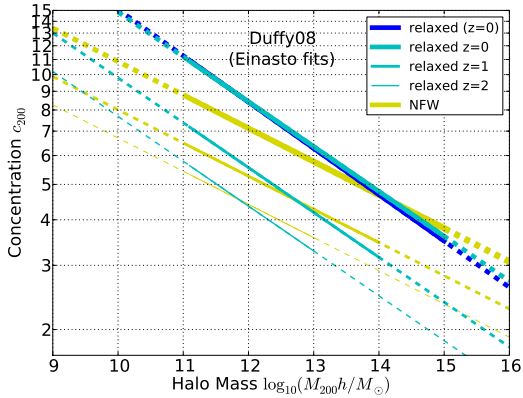


FIG. 8.— Expected concentrations derived from *Einasto* profiles compared to NFW profiles. Plotted are relations for relaxed halos from Duffy et al. (2008). The yellow NFW lines were plotted in Fig. 3.

TABLE 7
SIMULATIONS

Simulation	Cosmology (see Table 8)	M_{\min} [$h^{-1}M_{\odot}$]	M_{\max} [$h^{-1}M_{\odot}$]	N all	N relaxed	particles within r_{vir}
Duffy08	WMAP5	10^{11}	10^{15}	1,269	561	10,000
Maccio08	WMAP5	10^{10}	10^{15}	9,988	7,060	500
Neto07 (Millennium)	WMAP1	10^{12}	10^{15}	53,626	39,330	10,000
Hennawi07	WMAP1	10^{14}	10^{15}	878
Bullock01	WMAP1	10^{11}	10^{14}	$\sim 5,000$...	150–120,000
Gentile07 (NFW96)	WMAP3	3×10^{11}	3×10^{15}	19	...	5,000–10,000

TABLE 8
COSMOLOGICAL PARAMETERS

Author	WMAP	Ω_m	σ_8
Bullock01	WMAP1	0.3	1.0
Hennawi07	WMAP1	0.3	0.95
Neto07: Millennium	WMAP1	0.25	0.90
Maccio08	WMAP1	0.268	0.90
Maccio08	WMAP3	0.238	0.75
Maccio08, Duffy08	WMAP5	0.258	0.796
...	WMAP7	0.26	0.803

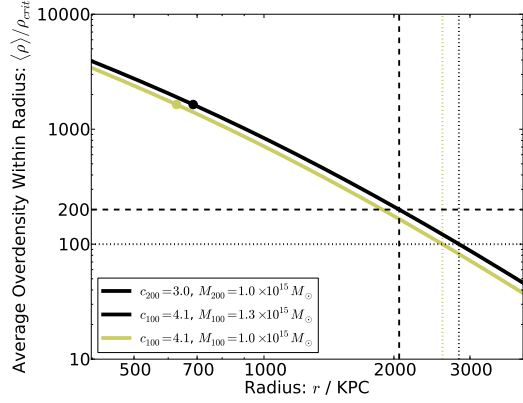


FIG. 9.— For a fixed NFW curve (r_s, ρ_s), illustration of conversion of (c, M) between different values of Δ_c . From Fig. 11, we find $c_{100} \approx 1.37c_{200}$ and $M_{100} \approx 1.3M_{200}$. The two (perfectly overlapping) black curves have identical (r_s, ρ_s) . Dots mark r_s , while the dashed lines mark the overdensities and r_{vir} for $\Delta_c = 200$ and 100. Note that for fixed c , r_s and r_{vir} vary with M_{vir} (black vs. yellow).

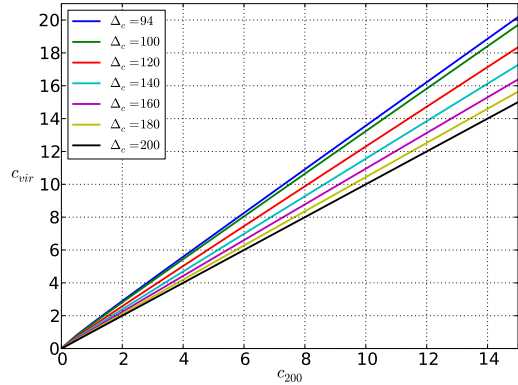


FIG. 10.— Conversion from NFW c_{200} to c_{vir} for $\Delta_c = 94, 100, 120, 140, 160, 180, 200$. The relations are extremely linear for $c_{200} > 2$.

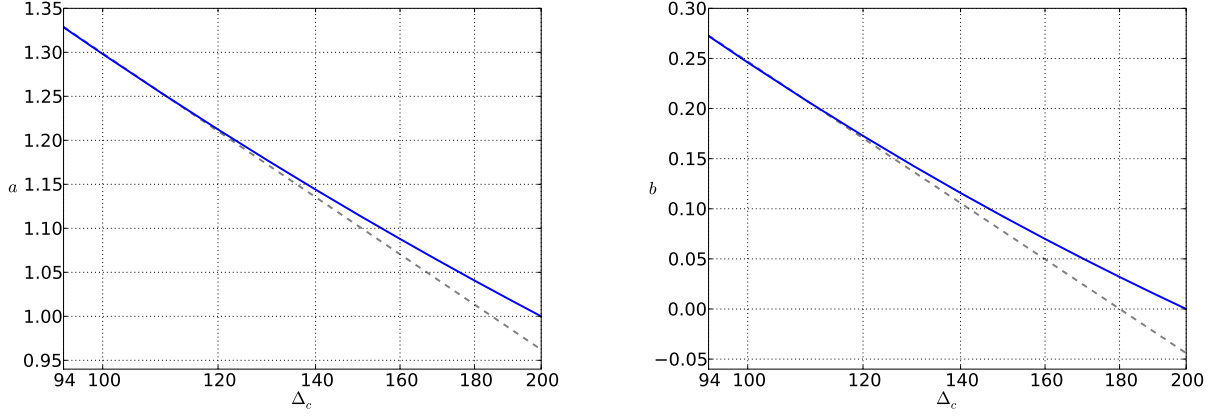


FIG. 10.— Parameters a and b for conversion of NFW $c_{vir} \approx a c_{200} + b$. Dashed lines are the relations given in Eqs. 19 & 20.

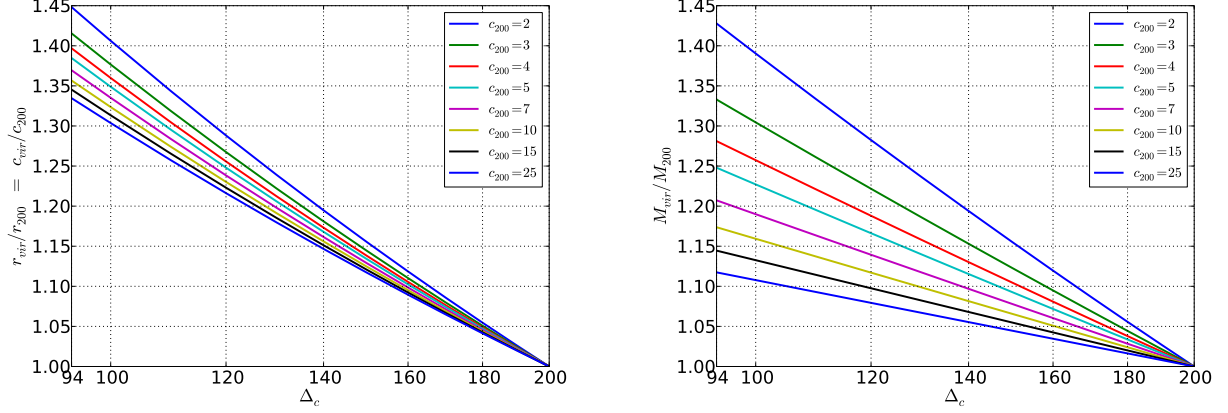


FIG. 11.— Ratios of r_{vir} (left) and M_{vir} (right) to the $\Delta_c = 200$ values as a function of NFW (c , Δ_c). Note that $r_{vir}/r_{200} = c_{vir}/c_{200}$ since we hold r_s (and ρ_s) fixed and we define $r_{vir} = c_{vir} r_s$ and $r_{200} = c_{200} r_s$.

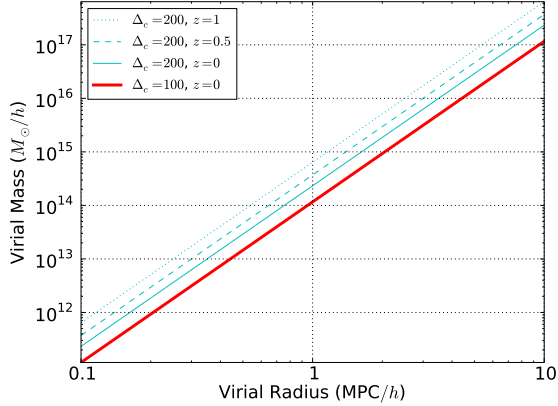


FIG. 12.— The relation between r_{vir} and M_{vir} is independent of the assumed profile, only dependent on the chosen overdensity, cosmology, and halo redshift (Eq. 23). For a $z = 0$ halo with $r_{vir} = 1$ Mpc/h, $M_{vir} = 1.16 \times 10^{14} M_{\odot}/h$ ($\Delta_c/100$).

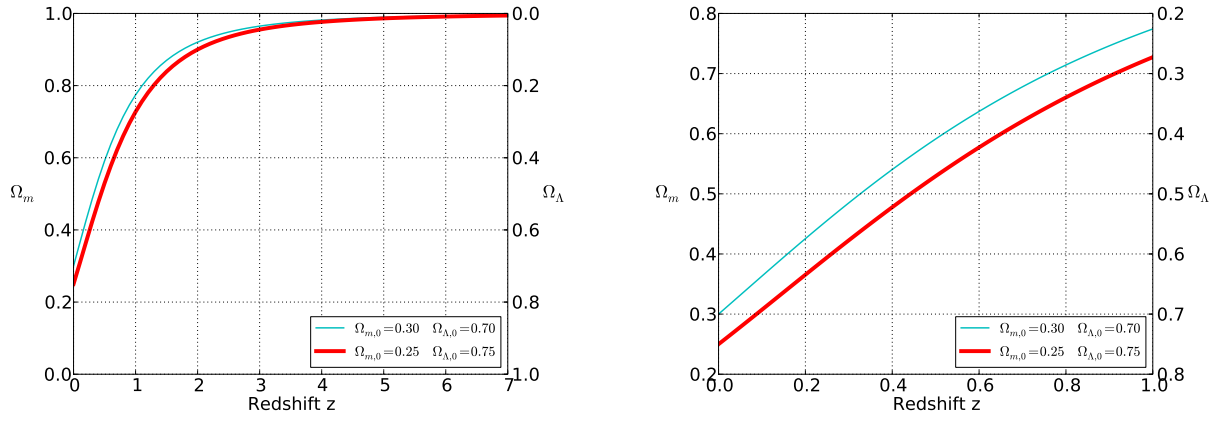


FIG. 13.— $\Omega_m(z) = 1 - \Omega_\Lambda(z)$ in a flat universe with a cosmological constant

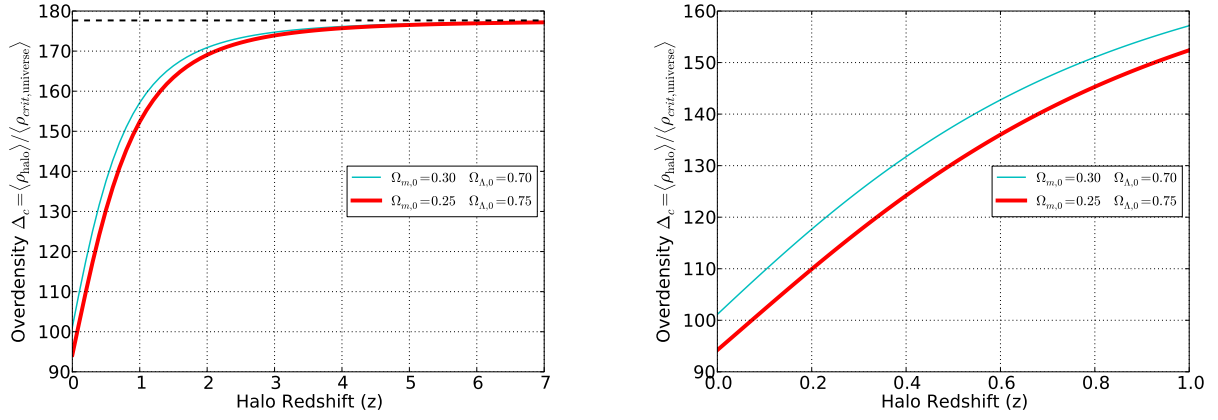


FIG. 14.— $\Delta_c(z)$: The average overdensity above ρ_{crit} within a collapsed halo

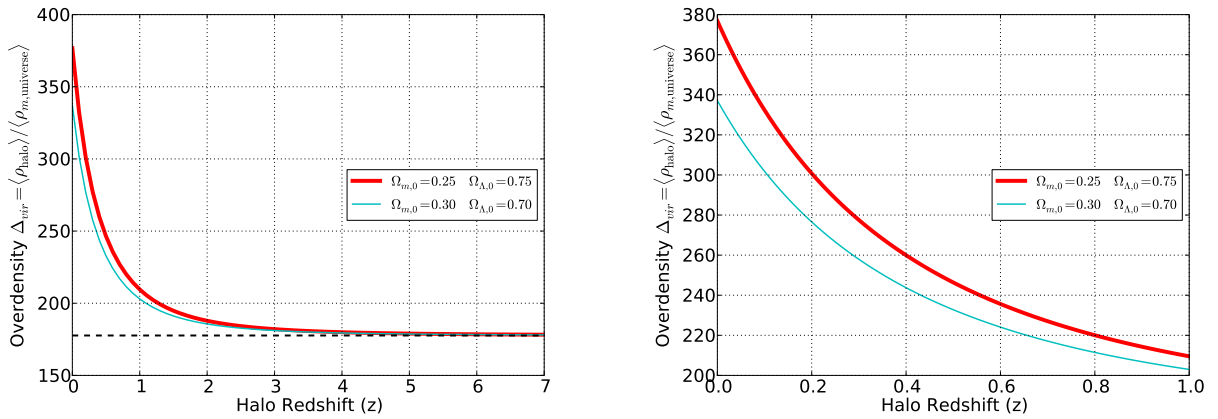


FIG. 15.— $\Delta_{\text{vir}}(z)$: The average overdensity above $\rho_m = \Omega_m \rho_{\text{crit}}$ within a collapsed halo

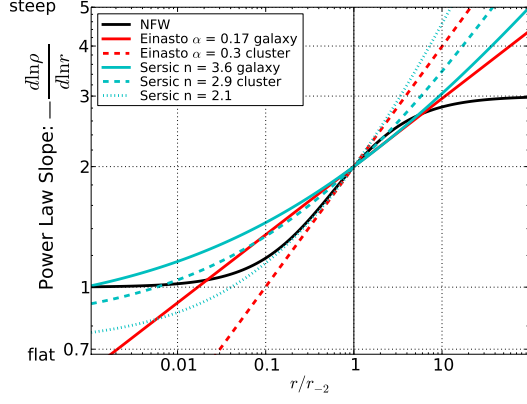


FIG. 16.— Power law slopes γ' for 3-D density $\rho \propto r^{-\gamma'}$. Here we compare the NFW, Einasto, and Sérsic profiles. For Sérsic we use the Prugniel-Simien approximation. A realistic range of α and n are plotted for the profiles, as found in simulations (Merritt et al. 2006; Gao et al. 2008; Navarro et al. 2010).

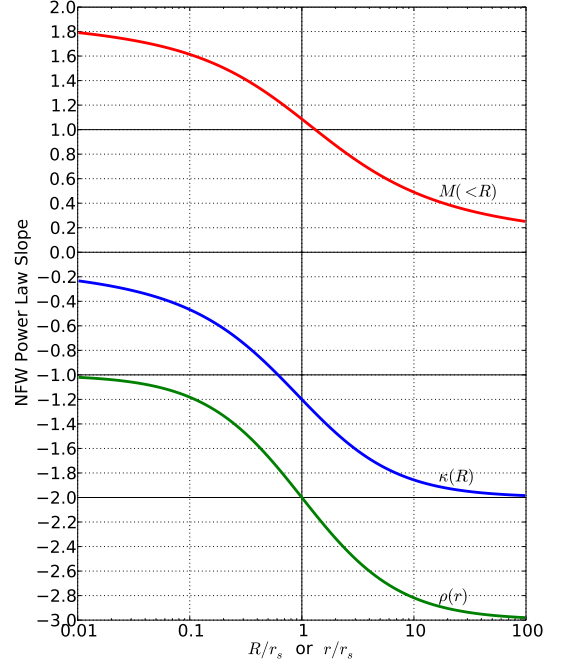


FIG. 19.— NFW power law slopes for projected mass within a cylinder $M(< R)$, projected mass density $\kappa(R)$, and 3-D density $\rho(r)$.

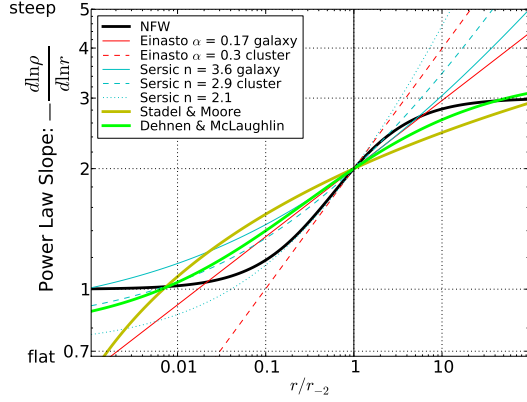


FIG. 17.— Power law slopes γ' for 3-D density $\rho \propto r^{-\gamma'}$. In this figure we add the Dehnen-McLaughlin and Stadel-Moore profiles with $\gamma = 7/9$ and $\lambda = 0.10$, respectively.

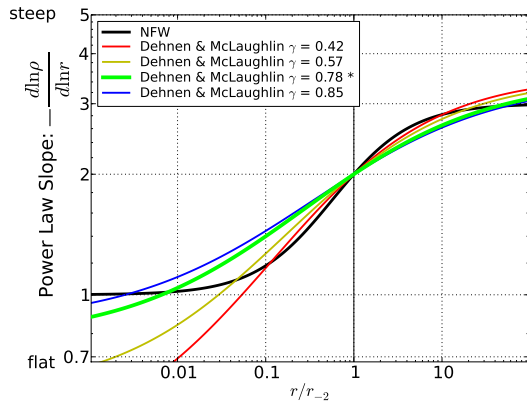


FIG. 18.— Power law slopes γ' for 3-D density $\rho \propto r^{-\gamma'}$. Here we compare various values of γ for Dehnen-McLaughlin as observed in simulations (Merritt et al. 2006). The value marked with a * ($7/9$) is used in their 2-parameter fitting formula.

REFERENCES

- Alam, S. M. K., Bullock, J. S., & Weinberg, D. H. 2002, *ApJ*, 572, 34 [ADS]
- Barkana, R. & Loeb, A. 2009, *ArXiv e-prints* [ADS]
- Broadhurst, T., Benítez, N., Coe, D., Sharon, K., Zekser, K., White, R., Ford, H., Bouwens, R., et al. 2005a, *ApJ*, 621, 53 [ADS]
- Broadhurst, T., Takada, M., Umetsu, K., Kong, X., Arimoto, N., Chiba, M., & Futamase, T. 2005b, *ApJ*, 619, L143 [ADS]
- Broadhurst, T., Umetsu, K., Medezinski, E., Oguri, M., & Rephaeli, Y. 2008, *ApJ*, 685, L9 [ADS]
- Bryan, G. L. & Norman, M. L. 1998, *ApJ*, 495, 80 [ADS]
- Bullock, J. S., Kolatt, T. S., Sigad, Y., Somerville, R. S., Kravtsov, A. V., Klypin, A. A., Primack, J. R., & Dekel, A. 2001, *MNRAS*, 321, 559 [ADS]
- Buote, D. A., Gastaldello, F., Humphrey, P. J., Zappacosta, L., Bullock, J. S., Brighenti, F., & Mathews, W. G. 2007, *ApJ*, 664, 123 [ADS]
- Cardone, V. F. 2004, *A&A*, 415, 839 [ADS]
- Coe, D. A., Benítez, N., Broadhurst, T., & Moustakas, L. A. Ford, H. 2010, *ArXiv Astrophysics e-prints*
- Cole, S. & Lacey, C. 1996, *MNRAS*, 281, 716 [ADS]
- Comerford, J. M. & Natarajan, P. 2007, *MNRAS*, 379, 190 [ADS]
- Dehnen, W. & McLaughlin, D. E. 2005, *MNRAS*, 363, 1057 [ADS]
- Dhar, B. K. & Williams, L. L. R. 2010, *MNRAS*, 480 [ADS]
- Diemand, J., Zemp, M., Moore, B., Stadel, J., & Carollo, C. M. 2005, *MNRAS*, 364, 665 [ADS]
- Dolag, K., Bartelmann, M., Perrotta, F., Baccigalupi, C., Moscardini, L., Meneghetti, M., & Tormen, G. 2004, *A&A*, 416, 853 [ADS]
- Duffy, A. R., Schaye, J., Kay, S. T., & Dalla Vecchia, C. 2008, *MNRAS*, 390, L64 [ADS]
- Dutton, A. A., van den Bosch, F. C., Dekel, A., & Courteau, S. 2007, *ApJ*, 654, 27 [ADS]
- Einasto, J. 1965, *Trudy Inst. Astroz. Alma-Ata*, 51, 87
- Eke, V. R., Navarro, J. F., & Frenk, C. S. 1998, *ApJ*, 503, 569 [ADS]
- Eke, V. R., Navarro, J. F., & Steinmetz, M. 2001, *ApJ*, 554, 114 [ADS]
- Elíasdóttir, Á. & Möller, O. 2007, *Journal of Cosmology and Astro-Particle Physics*, 7, 6 [ADS]
- Gao, L., Navarro, J. F., Cole, S., Frenk, C. S., White, S. D. M., Springel, V., Jenkins, A., & Neto, A. F. 2008, *MNRAS*, 387, 536 [ADS]
- Gentile, G., Tonini, C., & Salucci, P. 2007, *ArXiv Astrophysics e-prints* [ADS]
- Gnedin, O. Y., Weinberg, D. H., Pizagno, J., Prada, F., & Rix, H. 2007, *ApJ*, 671, 1115 [ADS]
- Golse, G. & Kneib, J.-P. 2002, *A&A*, 390, 821 [ADS]
- Graham, A. W. & Driver, S. P. 2005, *Publications of the Astronomical Society of Australia*, 22, 118 [ADS]
- Graham, A. W., Merritt, D., Moore, B., Diemand, J., & Terzić, B. 2006, *AJ*, 132, 2701 [ADS]
- Grossi, M. & Springel, V. 2009, *MNRAS*, 394, 1559 [ADS]
- Hayashi, E. & White, S. D. M. 2008, *MNRAS*, 388, 2 [ADS]
- Hennawi, J. F., Dalal, N., Bode, P., & Ostriker, J. P. 2007, *ApJ*, 654, 714 [ADS]
- Henry, J. P. 2000, *ApJ*, 534, 565 [ADS]
- Hernquist, L. 1990, *ApJ*, 356, 359 [ADS]
- Hu, W. & Kravtsov, A. V. 2003, *ApJ*, 584, 702 [ADS]
- Johnston, D. E., Sheldon, E. S., Wechsler, R. H., Rozo, E., Koester, B. P., Frieman, J. A., McKay, T. A., Evrard, A. E., et al. 2007, *ArXiv e-prints* [ADS]
- Klypin, A., Kravtsov, A. V., Bullock, J. S., & Primack, J. R. 2001, *ApJ*, 554, 903 [ADS]
- Komatsu, E., Smith, K. M., Dunkley, J., Bennett, C. L., Gold, B., Hinshaw, G., Jarosik, N., Larson, D., et al. 2010, *ArXiv e-prints* [ADS]
- Kuhlen, M., Strigari, L. E., Zentner, A. R., Bullock, J. S., & Primack, J. R. 2005, *MNRAS*, 357, 387 [ADS]
- Lapi, A. & Cavaliere, A. 2009, *ApJ*, 695, L125 [ADS]
- Lu, Y., Mo, H. J., Katz, N., & Weinberg, M. D. 2006, *MNRAS*, 368, 1931 [ADS]
- Macciò, A. V., Dutton, A. A., & van den Bosch, F. C. 2008, *MNRAS*, 391, 1940 [ADS]
- Mandelbaum, R., Seljak, U., & Hirata, C. M. 2008, *Journal of Cosmology and Astro-Particle Physics*, 8, 6 [ADS]
- Meneghetti, M., Fedeli, C., Pace, F., Gottloeber, S., & Yepes, G. 2010, *ArXiv e-prints* [ADS]
- Merritt, D., Graham, A. W., Moore, B., Diemand, J., & Terzić, B. 2006, *AJ*, 132, 2685 [ADS]
- Merritt, D., Navarro, J. F., Ludlow, A., & Jenkins, A. 2005, *ApJ*, 624, L85 [ADS]
- Moore, B., Quinn, T., Governato, F., Stadel, J., & Lake, G. 1999, *MNRAS*, 310, 1147 [ADS]
- Nakamura, T. T. & Suto, Y. 1997, *Progress of Theoretical Physics*, 97, 49 [ADS]
- Navarro, J. F., Frenk, C. S., & White, S. D. M. 1996, *ApJ*, 462, 563 [ADS]
- . 1997, *ApJ*, 490, 493 [ADS]
- Navarro, J. F., Hayashi, E., Power, C., Jenkins, A. R., Frenk, C. S., White, S. D. M., Springel, V., Stadel, J., et al. 2004, *MNRAS*, 349, 1039 [ADS]
- Navarro, J. F., Ludlow, A., Springel, V., Wang, J., Vogelsberger, M., White, S. D. M., Jenkins, A., Frenk, C. S., et al. 2010, *MNRAS*, 402, 21 [ADS]
- Neto, A. F., Gao, L., Bett, P., Cole, S., Navarro, J. F., Frenk, C. S., White, S. D. M., Springel, V., et al. 2007, *MNRAS*, 381, 1450 [ADS]
- Oguri, M., Hennawi, J. F., Gladders, M. D., Dahle, H., Natarajan, P., Dalal, N., Koester, B. P., Sharon, K., et al. 2009, *ApJ*, 699, 1038 [ADS]
- Okabe, N., Takada, M., Umetsu, K., Futamase, T., & Smith, G. P. 2009, *ArXiv e-prints* [ADS]
- Peebles, P. J. E. 1980, *The large-scale structure of the universe* (Research supported by the National Science Foundation. Princeton, N.J., Princeton University Press, 1980. 435 p.) [ADS]
- Prugniel, P. & Simien, F. 1997, *A&A*, 321, 111 [ADS]
- Richard, J., Smith, G. P., Kneib, J., Ellis, R., Sanderson, A. J. R., Pei, L., Targett, T., Sand, D., et al. 2009, *ArXiv e-prints* [ADS]
- Riess, A. G., Macri, L., Casertano, S., Sosey, M., Lampeitl, H., Ferguson, H. C., Filippenko, A. V., Jha, S. W., et al. 2009, *ApJ*, 699, 539 [ADS]
- Schmidt, R. W. & Allen, S. W. 2007, *MNRAS*, 379, 209 [ADS]
- Sereno, M., Jetzer, P., & Lubini, M. 2010, *ArXiv e-prints* [ADS]
- Sérsic, J. L. 1968, *Atlas de galaxias australes* (Cordoba, Argentina: Observatorio Astronomico, 1968) [ADS]
- Shaw, L. D., Weller, J., Ostriker, J. P., & Bode, P. 2006, *ApJ*, 646, 815 [ADS]
- Spergel, D. N., Verde, L., Peiris, H. V., Komatsu, E., Nolta, M. R., Bennett, C. L., Halpern, M., Hinshaw, G., et al. 2003, *ApJS*, 148, 175 [ADS]
- Stadel, J., Potter, D., Moore, B., Diemand, J., Madau, P., Zemp, M., Kuhlen, M., & Quilis, V. 2009, *MNRAS*, 398, L21 [ADS]
- Terzić, B. & Graham, A. W. 2005, *MNRAS*, 362, 197 [ADS]
- Wechsler, R. H., Bullock, J. S., Primack, J. R., Kravtsov, A. V., & Dekel, A. 2002, *ApJ*, 568, 52 [ADS]
- Wyithe, J. S. B., Turner, E. L., & Spergel, D. N. 2001, *ApJ*, 555, 504 [ADS]
- Zhao, D. H., Jing, Y. P., Mo, H. J., & Börner, G. 2003, *ApJ*, 597, L9 [ADS]
- Zhao, H. 1996, *MNRAS*, 278, 488 [ADS]